s article has been accepted for publication in a future issue of this journal, but has not been fully edited. Content may change prior to final publication. Citation information: DOI 10.1109/TMBMC.2019.2955094, IE
Transactions on Molecular, Biological and Multi-Scale Communications

Experimental and Analytical Analysis of Macro-Scale Molecular Communications Within Closed Boundaries

Daniel Tunç McGuiness*, Stamatios Giannoukos*†, Stephen Taylor * and Alan Marshall*, *Senior Member, IEEE*
*Department of Electrical Engineering and Electronics University of Liverpool Liverpool UK
†Laboratory of Atmospheric Chemistry, Paul Scherrer Institute, 5232 Villigen, Switzerland

***Abstract*—Molecular communication (MC) is an emerging field where the transmission of information occurs using particles (i.e., molecules, pheromones) instead of electromagnetic (EM) waves. This change in propagation medium opens up new possibilities for MC in areas where EM is inefficient or impossible such as underwater and underground communications. This study reports transmission experiments conducted to analyze the propagation behaviour in a closed boundary. It is shown that the behaviour can be explained by using the advection-diffusion equation (ADE) where the diffusion parameter of the equation plays a pivotal role in the process of the propagation. The signal properties of the transmission are analyzed and modelled theoretically and it is shown that the communication exhibits complex behaviour for signal amplitude, signal energy and signal-to-noise ratio with respect to transmission distance.**

***Index Terms*—Macro-scale molecular communication, Closed Boundary, Mass Spectrometer.**

I. Introduction

FROM the mid 19^{th} century, the transmission of information has been dominated by the use of electromagnetic (EM) waves and current technologies such as the internet and mobile communications rely solely on EM propagation. Although EM based systems are established and well understood, there are areas where this type of communication is not suitable or possible. These include areas where the environment poses a challenge to signal propagation (i.e. underground [1], underwater [2], infastructure monitoring [3] etc.). In these scenarios, alternative types of communication would prove useful. Molecular communication (MC) is such an alternative where the information is propagated by particles (molecules) instead of EM waves [4]. It is also shown that MC has an advantage over EM communication in complex environments where multiple obstacles are present, where higher attenuation was observed in EM compared to MC [5].

The use of molecular communication can be seen on a wide scale in the animal and plant kingdoms. At smaller scales it can be seen in cell-to-cell communication such as cell signalling where cells communicate with their environment and respond temporally to external cues that they sense [6]–[9]. On larger scales it can be observed in animals, conveying information using complex molecules such as pheromones [10]–[12]. Moths are the usually cited example of this type of communication, as they utilize their antennas to detect pheromones over long distances. Previously given examples show that molecular communications can be utilized in large scales (cm - m) as well as small scales (nm - μm).

This change in how communication is achieved opens up new possibilities of usage. As mentioned, application areas include underground or underwater communications, such as mines [1] or underwater sensor networks [2] where the environment causes high attenuation and absorption of the signal [5], [13], [14]. Understanding of MC could find biomimetic applications such as the development of pheromone type communication used between robots [15]–[19].

In MC signal modulation, different parameters to EM communications are used and these may be classified into three major groups. The first group is where modulation is achieved by changing the molecular concentration values and assigning the concentrations to different symbols. Examples that utilize this property are On-Off Keying (OOK) and Concentration Shift Keying (CSK) [20]–[22]. The second group is the time of release where the symbols are defined by the time they are sent by the transmitter or received by the receiver. These include Pulse Amplitude Modulation (PAM) and Pulse Position Modulation (PPM) [23]–[25]. The third group is the particle type, where the type of the particle is used to define the symbol. These include isomer-based modulation methods such as Isomer Molecular Shift Keying (I-MoSK) or Isomer-Molecular Shift Keying (I-CSK) [20], [21], [26].

Based on these three methods a number of molecular modulation schemes have been experimentally studied. In [27] a proof-of-concept application was demonstrated by transmitting chemicals using OOK with a MQ3 sensor. By utilizing an Arduino based transmitter, droplets of chemicals can be transmitted and received over distances of up to 4m. However, such transmission relies on discrete pulsation of chemicals. An alternative to this method is the utilization of constant flow to be the carrier and send the chemicals via this carrier. Such a system was experimented in [28] where a mass spectrometer (MS) was used as a detector to study both OOK and CSK. However, molecular communication can also be realized by using organic elements. One such experimental study is [29] where the modulator of the chemicals are the bacteria *Escherichia coli*.

The way transmission is achieved in macro-molecular communications, can be grouped into two methods: diffusion [31]–[38] (passive) and advection [39]–[43] (active). There are advantages and disadvatages of using each. Relying on

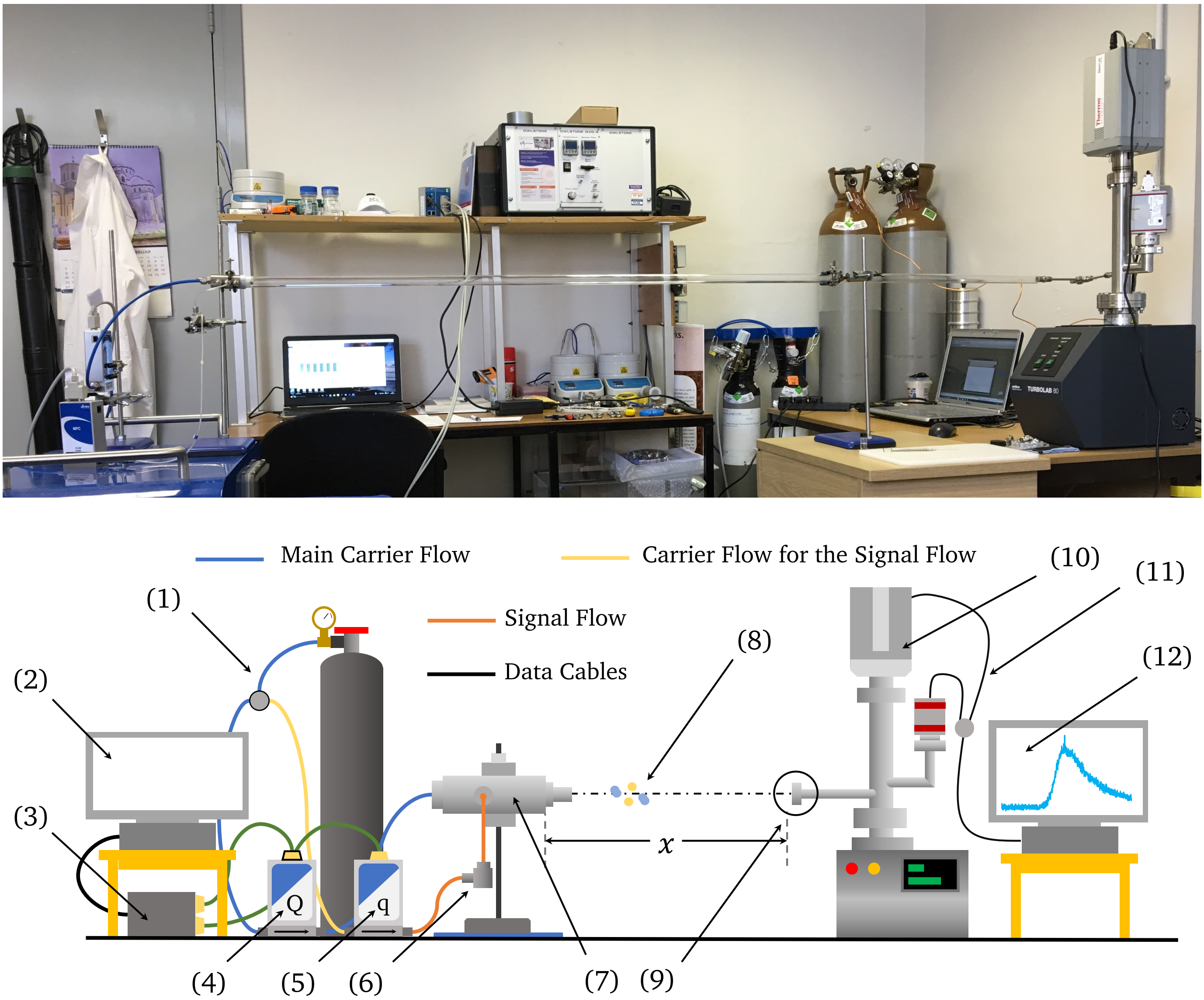

Fig. 1. **Upper image:** Experimental setup. **Lower image:** The diagram of the closed boundary experimental setup: **(1)** (N_2) gas is used as the carrier flow (Q) and is transferred into the MFC that control both the carrier flow (blue line) (Q) and the signal flow (yellow line) (q) **(2)** Modulation information is generated using a computer software **(3)** generated modulation is transmitted into an automation platform where it sends the modulation to the MFC's to create pulses **(4)** MFC for the carrier flow **(5)** MFC for the signal flow **(6)** Evaporation Chamber (EC) where the signal chemical is injected **(7)** Mixing chamber where the signal chemicals arrive and initiate the transmission from the transmitter to the detector **(8)** Semipermeable membrane present in the inlet of the mass spectrometer **(9)** the inlet of the mass spectrometer **(10)** electronics control unit (ECU) which controls the mass analyser **(11)** Data acquisition and analysis [30].

diffusion alone makes the transmission energy independent [4], however this makes the propagation random since the chemicals movement can be in any direction [44]. However propagation via diffusion can also be used in areas which can be a better method over EM which was studied in [5].

Using an advective flow forces the particles to move in the direction of the velocity vector but requires the communication to rely on external energy. Over distances of cm - m, relying on diffusion alone is not enough, making advection a necessity for macro-scale communications [30] which this study investigates as the main propagation method

In all previous studies, the propagation medium is chosen to be open space where the medium between the transmitter and the receiver has no boundary. While open transmission requires minimal environmental isolation, the transmission distance that can be achieved is limited, as shown in [45]. Closed boundary transmission opens up longer range of communication and the messenger chemical be protected from outside interferences and can be observed in natural processes such as delivery of particles in a blood stream or propagation of minerals from roots to leafs in plants (i.e., vascular system) [46]. A study conducted in [28] showed an experimental transmission of closed-boundary experiment. However, the

s article has been accepted for publication in a future issue of this journal, but has not been fully edited. Content may change prior to final publication. Citation information: DOI 10.1109/TMBMC.2019.2955094, IE
Transactions on Molecular, Biological and Multi-Scale Communications

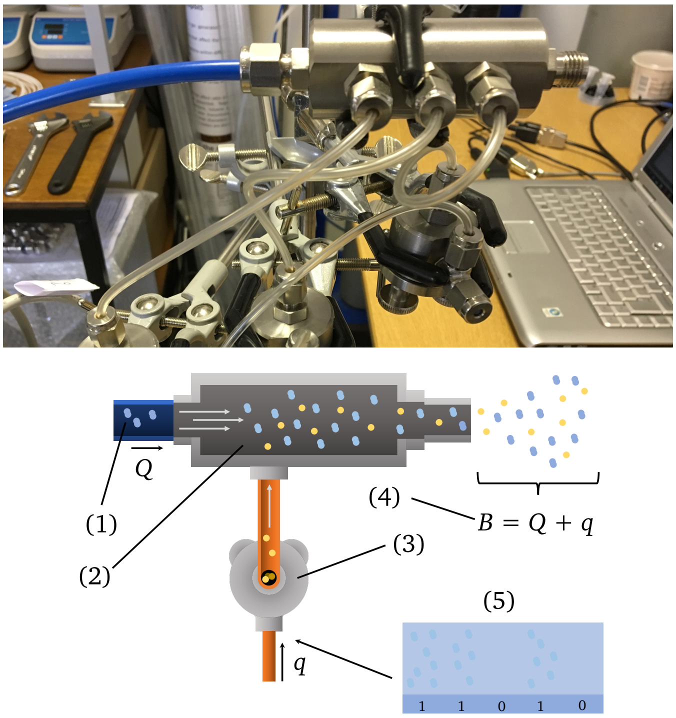

Fig. 2. **Upper image:** Evaporation Chamber. **Lower image:** The working diagram of the odour gas generator [47] **(1)** Carrier gas *(Q)* introduction into the mixing chamber **(2)** Mixing chamber **(3)** Evaporation chamber (Figure 3) **(4)** Transmitted chemicals that are released from the chamber. **(5)** A modulation sequence that is used to create gas pulses [30].

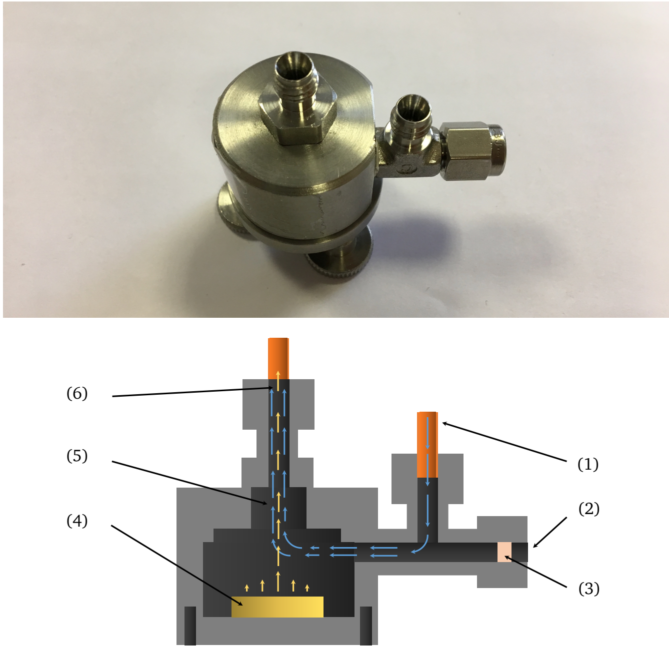

Fig. 3. **Upper image:** Evaporation Chamber. **Lower image:** Diagram of the evaporation chamber: **(1)** Inlet of the N_2 gas to the evaporation chamber **(2)** Sample introduction **(3)** thermo-resistant septum that lets multiple introduction of a sample introduction**(4)** An absorptive material that holds the sample **(5)** N_2 from the inlet carries the evaporated chemicals from the chamber **(6)** The cumulated gas it transferred into the mixing chamber via a 0.25 inch Teflon tube [30].

analysis of the study was more emphasized on the experimental compared to the mathematics of the propagation.

The contributions of the paper are as follows

- **Closed Boundary Experiment:** MC is a novel research topic with experimental work recently gaining momentum. This experimental test-bed provides an understanding into the behaviour of MC propagation inside a bounded domain. The knowledge gained from this experiment can be transferred into applications where MC propagation is done in closed environments. These include infrastructure monitoring where sensors can communicate through pipes. Closed boundary behaviour can also be used to study drug delivery in circulatory systems or molecular communication through established infrastructures (i.e., pipes)
- **Mathematical Modelling:** This paper provides a mathematical modelling that explains the behaviour of the propagation in a closed boundary.
- **Signal Characteristics:** The signal strength, signal energy and signal-to-noise ratio (SNR) are analyzed for each distance and compared to the developed theoretical model which is also presented in this paper.

The structure of the paper is as follows. Following this introduction (Section I), Section II describes the experimental test-bed used in this study. Section III considers the theoretical aspects of transmission of information by MC in a bounded medium. In Section IV, the experimental results are shown alongside the theoretical models developed in Section III and compared for transmitted signal, signal amplitude, signal energy, signal-to-noise ratio respectively with addition comparisons for different transmission medium radii. In Section V, conclusions of the study are discussed with suggested future-work.

II. Experimental Setup

To analyze closed boundary transmission and its effect on the propagation and signal delay, an experimental setup was created. To generate and to transmit the particles, an odor transmitter was developed [28], [30], [47]–[49]. To detect the sent particles and distinguish them, a membrane inlet mass spectrometer with a quadrupole mass analyzes (QMA) was used. Mass spectrometers are analytical instruments capable of distinguishing molecules in a given sample by analyzing the mass-to-charge ratios (m/z) [50]. A detailed diagram of the experimental setup can be seen in Figure 1.

A. Transmitter

The transmitter used in this experiment is an in-house built odor generator consisting of three major parts. The first part is made up from mass flow controllers (MFC) that based on the message, closes and opens the valves that control N_2 flow. This gas is then transferred into the second part of the transmitter, the evaporation chamber (EC). In here liquid analytes are introduced through a side injection port which is sealed off with a thermo-resistant septum. Here the injected chemicals are turned into the gas phase, due to being volatile organic compounds (VOCs), and with the aid of the N_2 flow

This article has been accepted for publication in a future issue of this journal, but has not been fully edited. Content may change prior to final publication. Citation information: DOI 10.1109/TMBMC.2019.2955094, IEEE Transactions on Molecular, Biological and Multi-Scale Communications

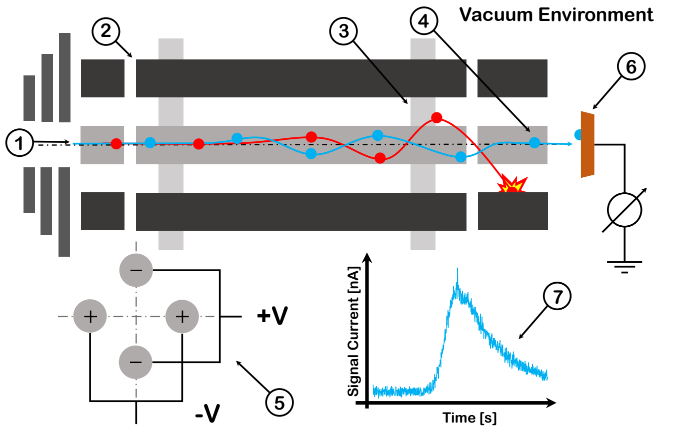

Fig. 4. Schematic diagram of the quadrupole mass analyzer used in the detection and identification of chemical analytes. **(1)** Samples are introduced into the QMA via the membrane inlet. The chemical analytes are ionized in the ion source and passed through a focus lens into the quadrupole analyser. **(2)** The analyzer is made up from four hyperbolic rods with applied RF and DC potentials. **(5)** Ions are separated based on their mass-to-charge values. Ions with stable trajectories, such as **(4)** will travel through the QMA and will arrive at the detector **(6)**, whereas ions with unstable trajectories (non-resonant ions), i.e. **(3)** will collide with the electrodes and will be filtered out from the detection. Detected ions are amplified and presented visually as mass chromatogram shown in **(7)**.

are carried from the evaporation chamber and into the mixing chamber. Here the chemicals are mixed, and with the presence of the carrier flow, are finally propelled from the transmitter to the transmission medium and into the detector. A detailed working diagram of both the transmitter and the evaporation chamber can be seen in Figures 2 and 3 respectively.

B. Detector

A portable membrane inlet mass spectrometer (MIMS), provided by Q technologies Ltd. was used as the detector for the experiments. The applications and the practice of the detector are described in literature in detail. [49], [51]–[55]. A MIMS consists of three primary parts: (a) the membrane sampling probe that allows the sample to pass from the outside environment and into the MS, (b) triple filter quadrupole mass spectrometer (QMS) which in itself consists of three parts: (b-1) electron ion source (EI), (b-2) mass analyzer and (b-3) detector and finally the last part of the detector is the (c) vacuum system. One of the defining features of the detector is the presence of the membrane, which greatly simplifies the introduction of the sample to the detector [56]. The membrane present in the detector is a fine non-sterile flat polydimethylsiloxane (PDMS) with a thickness of 0.12 mm and a sampling area of 0.32 mm^2 [49]. A diagram of a QMA can be seen in Figure 4.

C. Chemicals

In the following experiments two types of chemicals were used. To carry the chemicals from the evaporation chamber (EC) into the mixing chamber, and to create the necessary advective flow, zero-grade nitrogen gas (% 99.998 purity) was used. The signal chemical responsible for being the signal was chosen to be acetone (% 99.8 purity, CAS Number: 67-64-1), and methanol (over % 99.9 purity) was used as the dilution agent. N_2, supplied by BOC Ltd. was stored in gas phase and both methanol and acetone, supplied by Sigma-Aldrich were stored in liquid phase.

D. Transmission Medium

To study the effects of molecular communication transmission in a confined boundary, clear acrylic pipes were utilized. These pipes have an inner diameter of ϕ_{in} = 19.80 mm and an outer diameter of ϕ_{out} = 24.25 mm which these values can also be seen in Table II. The length (L) of these pipes ranges from 50 cm to 300 cm with 50 cm increments.

III. Transmission of Molecules in a Confined Medium

A. Advection-Diffusion Equation (ADE)

A communication that utilizes particles (i.e., molecules) as a means of transmission/propagation can be described using the continuity equation given below [57].

$$\frac{\partial c}{\partial t} + \nabla \cdot \mathbf{J} = K, \tag{1}$$

where the time derivative $(\partial c/\partial t)$ represents the accumulation or the loss of the mass present in the environment and the divergence term $(\nabla \cdot \mathbf{J})$ defines the difference between the flow going in and out of the environment. The flux present in the medium is made up from two types of sources. The former is the diffusive flux $(\mathbf{J}_{\mathrm{D}})$ caused by particle diffusion:

$$\mathbf{J}_{\mathrm{D}} = -D_m \nabla c, \tag{2}$$

whereas the latter is the flux $(\mathbf{J}_{\mathrm{A}})$ caused by the advective flow $(\mathbf{u})$.

$$\mathbf{J}_{\mathrm{A}} = \mathbf{u}\,, \tag{3}$$

By combining the fluxes described in Eq. (2) and Eq. (3) and substituting this term to Eq. (1) the the general expression of the Advective-Diffusion Equation (ADE) can be derived [58]:

$$\frac{\partial c}{\partial t} = -\nabla \cdot (\mathbf{J}_{\mathrm{A}} + \mathbf{J}_{\mathrm{D}}) + K, \tag{4a}$$
$$\frac{\partial c}{\partial t} = D_m \nabla^2 c - \nabla \cdot (\mathbf{u} c) + K, \tag{4b}$$

where c is the concentration in a given space and time $(\mathrm{kg/m^3})$, D_m is the coefficient of diffusion $(\mathrm{m^2/s})$, t is the transmission time (s), $\mathbf{u}$ is the advective flow $(\mathrm{m/s})$ and K is the sink and/or the source. Based on this expression given in Eq. (4b), the solution can be found by giving the equation initial conditions. The prototypical solution for this problem is the instantaneous injection of a mass (M) into the environment. This is also known as the “thin-film” solution in the literature [59]. The initial conditions for the ADE are as follows:

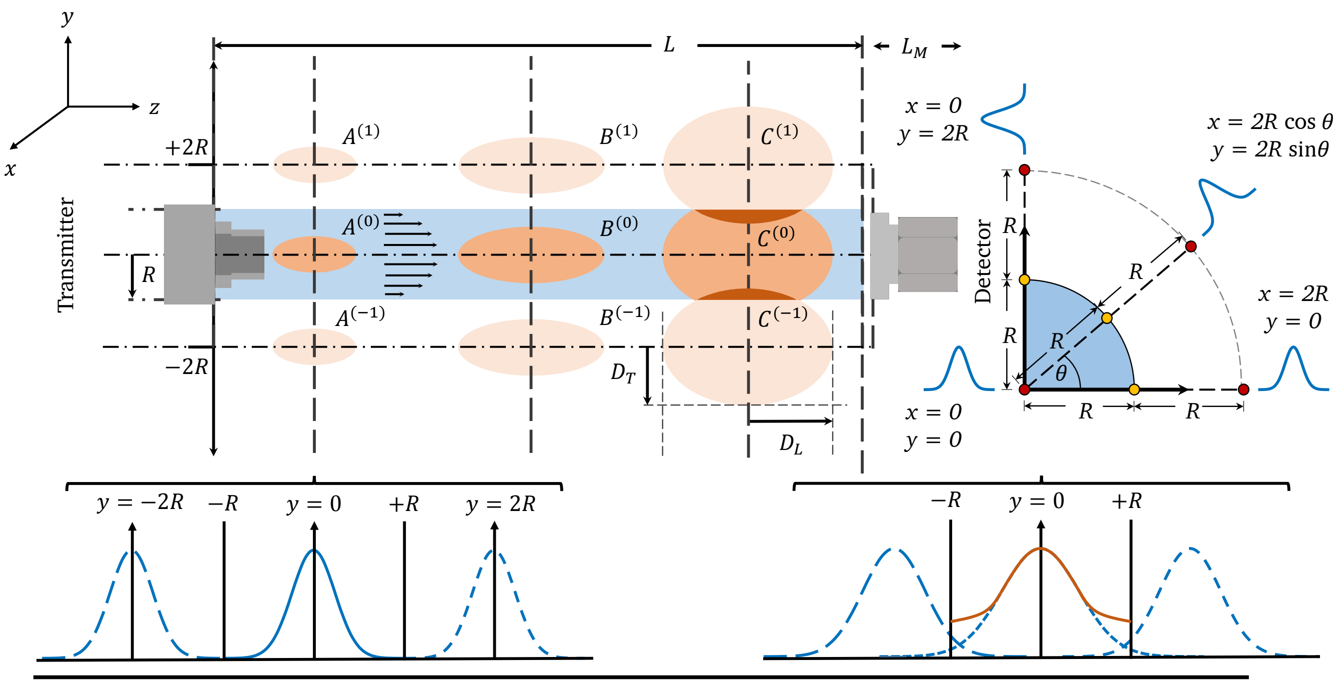

Fig. 5. A descriptive diagram of the model used in the study. At the initial stage of the experiment (t = 0 s) a mass is injected into the environment. This is represented as a Dirac delta function $\delta(x)$. Once the mass is injected, to simulate the effect of physical boundary of the environment ($A^{(0)}$), additional gas pulses are generated in the y-coordinates with positive sides being $y = 2L$, $y = 4R$, ..., $y = 2aR$ ($A^{(1,2,..,\infty)}$) and negative sides being $y = -2R$, $y = -4R$, ..., $y = -2nR$ ($A^{(-1,-2,..,-\infty)}$). This is also carried out in the z-coordinates with the parameter a. As transmission evolves the gas pulses transcends the boundary of the propagation medium, at which point the mirror pulses are added to the actual transmission to create the effect of the boundary.

$$c(|x| > 0,\, |y| > 0,\, |z| > 0,\, t = 0) = 0, \tag{5a}$$
$$c(x = 0,\, y = 0,\, z = 0,\, t = 0) = M\,\delta(x)\,\delta(y)\,\delta(z), \tag{5b}$$
$$c(|x| \to \infty,\, |y| \to \infty,\, |z| \to \infty,\, t) = 0. \tag{5c}$$

where $\delta(\cdot)$ denotes the dirac delta function. Based on this initial conditions, the solution for 3D space can be derived as follows:

$$c(x,\, y,\, z,\, t) = \frac{M}{\sqrt{(4\pi t)^3 D_x D_y D_z}} \times \exp\left(-\frac{(x-u_x t)^2}{4D_x t} - \frac{(y-u_y t)^2}{4D_y t} - \frac{(z-u_z t)^2}{4D_z t}\right), \tag{6}$$

where $(D_x,\, D_y,\, D_z)$ are diffusion coefficients of their respective dimensions $(\mathrm{m}^2/\mathrm{s})$ and $(u_x,\, u_y,\, u_z)$ are the advective flow in x, y and z dimensions respectively $(\mathrm{m/s})$. The following subsection will focus on deriving the radial-ADE.

B. The Radial-Advective-Diffusion Equation

Eq. (6) represents the concentration function in 3D Cartesian space and to describe the cylindrical geometry of the transmission medium, the equation is converted to cylindrical coordinates with the following transformations:

$$x = r\cos\theta \quad y = r\sin\theta \quad z = z, \tag{7a}$$
$$D_x = D_y = D_r \quad D_z = D_L, \tag{7b}$$
$$u_x = u_y = u_r \quad u_z = u_z. \tag{7c}$$

Following these conversion process, Eq. (6) can be written in its cylindrical form:

$$c(r,\, \theta,\, z,\, t) = \frac{M}{\sqrt{(4\pi D_r^2 D_z t)^3}} \exp\left(-\frac{(r\cos\theta - u_r t)^2}{4D_r t} - \frac{(r\sin\theta - u_r t)^2}{4D_r t} - \frac{(z-u_z t)^2}{4D_z t}\right). \tag{8}$$

This equation can be further simplified by using trigonometric identities (i.e., $r^2 = r^2\cos^2\theta + r^2\cos^2\theta$) and omitting the radial advective flow u_r to the following expression:

$$c(r,\, z,\, t) = \frac{M}{\sqrt{(4\pi D_r^2 D_z t)^3}} \exp\left(-\frac{r^2}{4D_r t} - \frac{(z-u_z t)^2}{4D_z t}\right). \tag{9}$$

1) Boundary Conditions: To create a boundary condition for this function, method of mirror images is used. This is a mathematical tool for solving PDE's by adding the mirror image of the function with respect to the symmetry hyperplane. For example to have a boundary at $x = x_0$ in 1D, the same function is added at $x = 2x_0$. This ensures that the change of concentration at the defined boundary x_0 equal to zero (i.e., zero flux at the radial boundary of the pipe). However, as the transmission evolves, more images are needed to maintain the accuracy of the function. Therefore, continuing the example, mirror images are added at distances $x = 4x_0$, $x = 6x_0$, ...

In the environment used in this study, there is only the radial no-flux boundary at R, where R is the radius of the boundary (m). If the transmission of particles are assumed to be in z-direction, the boundary condition can be expressed as:

$$\left.\frac{\partial c}{\partial r}\right|_{r=R} = 0. \tag{10}$$

2) Absorption/Desorption Process: Based on the boundary condition described in Eq. (10), the mirror functions can be implemented to the concentration function in 3D which is given as:

$$c(r,\, z,\, t) = \frac{M}{\sqrt{(4\pi t)^3 D_r^2 D_z}} \sum_{n=0}^{\infty} \exp\left(- \frac{(r-2nR)^2}{4D_r t} - \frac{(z-u_z t)^2}{4D_z t} \right) \tag{11}$$

where n is the number of mirror functions. As can be seen in the equation above, the function is independent from θ as it possesses angular symmetry. By integrating the concentration function with respect to the cylindrical volume element the particles that are present in the environment, (θ_E) can be calculated.

$$\theta_E = \iiint_V c\, dz\, r\, dr\, d\theta \tag{12}$$

As the system has no sink/source ($K = 0$), the chemicals that are used in the transmission can either be in the environment (θ_E) or have been absorbed by the detector (θ_A). Therefore, both the aforementioned mass values must add upto the initial introduction of mass in the beginning of the transmission.

$$M = \theta_E + \theta_A \tag{13}$$

The mass absorbed by the detector (θ_A), can be calculated by substracting from the inital mass (M) [30], [45].

$$\theta_A(r,\, \theta,\, z,\, t) = M - \theta_E(r,\, \theta,\, z,\, t) \tag{14a}$$

$$\theta_A(r,\, \theta,\, z,\, t) = M - \int_0^{2\pi}\int_0^{R}\int_0^{L} c(r,\, \theta,\, z,\, t)\, dz\, r\, dr\, d\theta \tag{14b}$$

where L is the distance between the transmitter and the detector (m). The solution to this equation, which expresses the absorbed particles by the detector, can be expressed as:

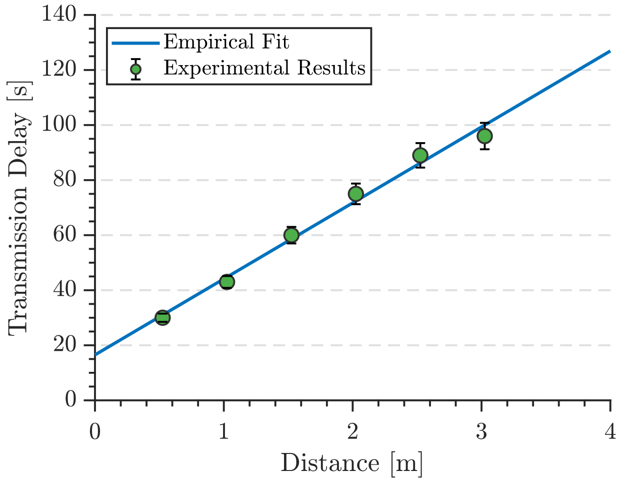

Fig. 6. Experimentally measured chemical detection with comparison to empirical fitting ($R^2 = 0.9891$).

$$\begin{aligned}\theta_A(R,\, L,\, t) &= M - \frac{M}{\mathbf{i}\sqrt{4D_T t}} \times \left[\operatorname{erf}\left(\frac{u_z t}{\sqrt{4D_L t}}\right) + \operatorname{erf}\left(\frac{L-u_z t}{\sqrt{4D_L t}}\right)\right] \\ &\sum_{n=0}^{\infty} \exp\left(-n^2\frac{R^2}{D_T t}\right)\left\{\mathbf{i}\sqrt{D_T t}\left[1-\exp\left((4n-1)\frac{R^2}{4D_T t}\right)\right] + nR\sqrt{\pi}\exp\left(n^2\frac{R^2}{D_T t}\right) \right. \\ &\left. \times \left[\operatorname{erfi}\left(n\frac{\mathbf{i}R}{\sqrt{D_T t}}\right) - \operatorname{erfi}\left(\frac{(2n-1)}{2}\frac{\mathbf{i}R}{\sqrt{D_T t}}\right)\right]\right\}\end{aligned} \tag{15}$$

where $\mathbf{i}$ is the imaginary unit with the identity $\mathbf{i}^2 = -1$ and $\operatorname{erfi}(\cdot)$ is the imaginary error function with the following identity.

$$\operatorname{erfi}(x) = -\mathbf{i}\operatorname{erf}(\mathbf{i}x) = \frac{2}{\sqrt{\pi}}\int_0^x e^{t^2}\, dt \tag{16}$$

Once the chemicals are absorbed by the detector, the removal process can be initiated. To begin the calculation of the desorption process the particles that have been absorbed needs to be quantified. To achieve this, the travel time of the signal has to be taken into account. As the chemical travels long distances, the response time is also delayed considerably and therefore the removal of particles from the detector to the outside environment is also delayed by the same amount of time. Therefore the particles that are absorbed by the detector the instant flush takes effect (M_R) can be calculated as:

$$M_R = \theta_A(R,\, L,\, T_S + t_{\text{emp}}) - \theta_A(R,\, L,\, t_{\text{emp}}) \tag{17}$$

where the T_S is the symbol period (s) and t_{emp} is the empirically measured time for the detection of chemical with respect to distance. The emprical fitting of this equation is given below and the fitting process can be seen in Figure 6.

s article has been accepted for publication in a future issue of this journal, but has not been fully edited. Content may change prior to final publication. Citation information: DOI 10.1109/TMBMC.2019.2955094, IE
Transactions on Molecular, Biological and Multi-Scale Communications

$$t_{\text{emp}}\left(L\right) = p_1 L + p_2 \tag{18a}$$

$$p_1 = 27.6 \qquad p_2 = 16.51 \tag{18b}$$

where p_1 and p_2 are the fitting parameters to the empirical fitting function. This parameter would change depending on the chemical that is used for sending information and in this study the function is based on Acetone being the signal chemical. Based on these preliminary definitions, the removal of particles from the detector to the outside environment can be defined as the following function [30]

$$\begin{aligned}\theta_D(R,\, L_M,\, t) = {} & \frac{M_R}{\mathbf{i}\sqrt{4D_T t}} \\ & \times \left[\operatorname{erf}\left(\frac{v_z t}{\sqrt{4D_L t}}\right) + \operatorname{erf}\left(\frac{L_M - v_z t}{\sqrt{4D_L t}}\right)\right] \\ \sum_{n=0}^{\infty} \exp\left(-n^2 \frac{R^2}{D_T t}\right) & \left\{\mathbf{i}\sqrt{D_T t}\left[1 - \exp\left((4n-1)\frac{R^2}{4D_T t}\right)\right]\right. \\ & + nR\sqrt{\pi}\exp\left(n^2\frac{R^2}{D_T t}\right) \\ & \left.\times\left[\operatorname{erfi}\left(n\frac{\mathbf{i}R}{\sqrt{D_T t}}\right) - \operatorname{erfi}\left(\frac{(2n-1)}{2}\frac{\mathbf{i}R}{\sqrt{D_T t}}\right)\right]\right\}\end{aligned} \tag{19}$$

where L_M is the distance between the membrane and the detector (m). It must be noted that unlike the absorption process, where chemicals travel long distance to reach the detector, in the desorption process the chemical propagation begins from the detector membrane and end at the outside environment ($L \gg L_M$). A detailed description of introduction/removal of particles can be seen in [30], [42] and a diagram of the model used in the study is presented in Figure 5.

C. *Calculation of the coefficient of Diffusivity*

To calculate the longitudinal diffusivity coefficient of the propagation (D_L), which plays a pivotal role in this type of communication transmission, the characteristic properties of the fluid motion must be established.

In a communication where particles are propagated through a medium, the main propeller of these particles are the volumetric flow rate (Q). This is defined as the amount of volume transported in a given amount of time (m^3/s) and the velocity parameter (u) can be obtained by dividing the volumetric flow rate by the cross-sectional area of the tube (A).

$$u_0 = \frac{Q}{A} = \frac{Q}{4\pi R^2} \qquad \overline{u} = \frac{1}{2}u_0 \tag{20}$$

After obtaining the velocity parameter, the next characteristic of a fluid motion to be established is whether the motion is laminar or turbulent. To calculate this value, the Reynolds number (Re) is used. The equation for Reynolds number can be seen below [60].

$$\mathrm{Re} = \overline{u}\frac{D}{\nu} \tag{21}$$

where, $\overline{u}$ is the mean velocity of the fluid (m/s), D is the diameter of the pipe (m) and ν is the kinematic viscosity of the fluid (m^2/s).

1) Entrance Length: Entrance length is defined as the distance a flow travels after entering a pipe before the flow becomes fully developed. Since the Reynolds number is low (Re $<$ 2000) the flow can be considered laminar and the entrance length for the system is calculated by the the following equation.

$$L_E = 0.05\, D\, \mathrm{Re} \tag{22}$$

2) Longitudinal Diffusivity: Longitudinal diffusivity is defined as diffusion paralel to the advective vector. As the flow is laminar (Re $<$ 2000) the longitudinal diffusivity can be calculated as:

$$D_L = D_m + \left(\frac{\overline{u}^2 R^2}{48 D_m}\right), \tag{23}$$

where D_m is the molecular diffusion (cm^2/s). The derivation of this equation can be seen in Appendix.

3) Transverse Diffusion: The presence of the membrane affects the transverse diffusion more profoundly than longitudinal since the main propagator of motion in radial axis is diffusion rather that advection aided diffusion seen in longitudinal diffusion. To calculate the coefficient, Einstein's equation is used.

$$\lim_{t\to\infty}\frac{d}{dt}\sum_{i=1}^{N}\frac{1}{6N}\{[r_i(t) - r_i(0)]\} \tag{24}$$

where $r_i(0)$ is the initial position coordinate of the gas molecules and $r_i(t)$ is the position coordinate of the gas molecule after time t.

TABLE I
CALCULATED AND USED PARAMETERS IN THE STUDY

Property	Symbol	Value	Unit
Mean velocity of the fluid	$\overline{u}$	2×10^{-2}	m/s
Diameter of the pipe	D	2×10^{-2}	m
Kinematic viscosity of the fluid[1]	ν	14×10^{-6}	m^2/s
Reynolds Number	Re	28	-
Laminar Diffusion	D_L	0.7679	cm^2/s
Transverse Diffusion	D_T	1×10^{-4}	cm/s^2
Volumetric Flow Rate	Q	750	ml/min
Injected Mass	M	0.325	ng

[1] Normal Temperature and Pressure

IV. EXPERIMENTAL RESULTS

In this study the effects of long distance transmission of molecular communication in a closed boundary is studied.

The parameters used in this experiment can be seen in Table II.

In this experiment 6 distances were studied, ranging from 0.5 m to 3.0 meter with increments 0.5 m.

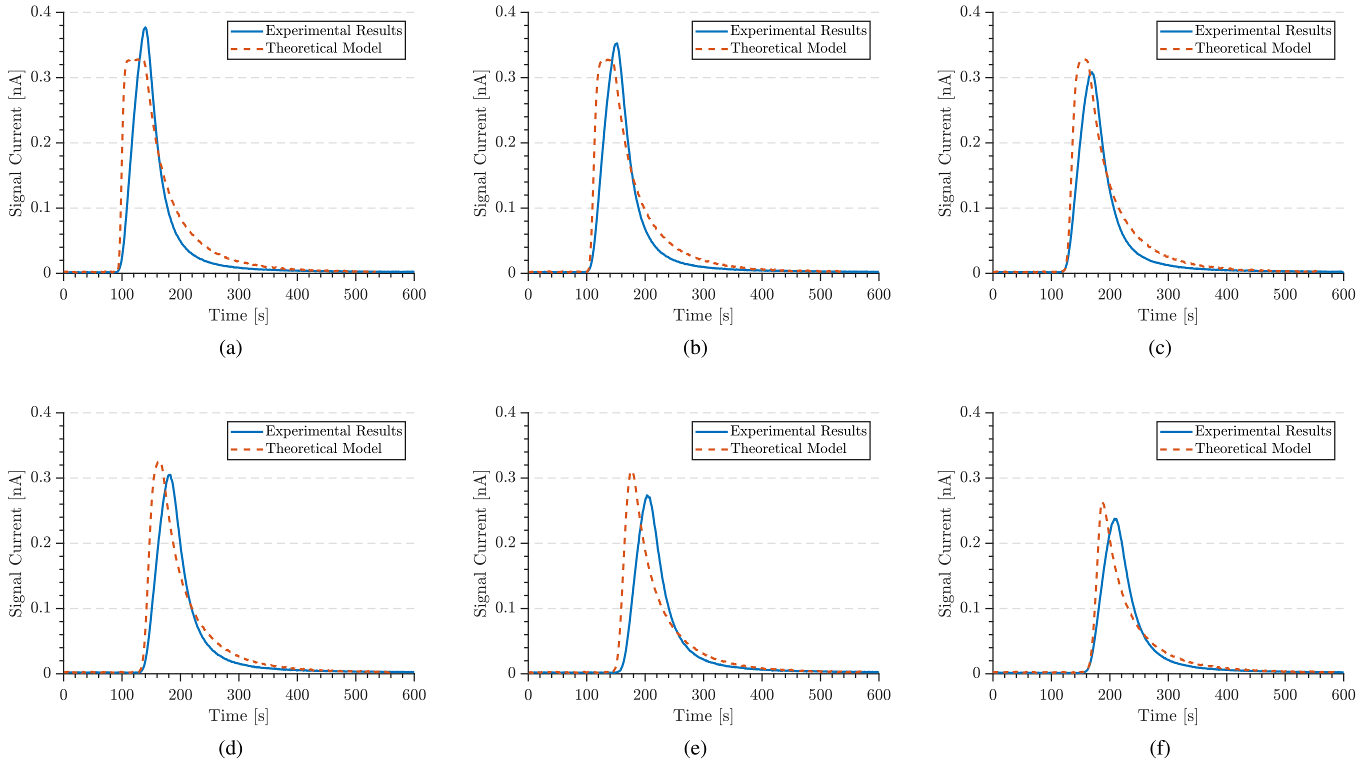

Fig. 7. Experimental along with theoretical comparison of each experimental transmission **(a)** 0.5 m **(b)** 1 m **(c)** 1.5 m **(d)** 2 m **(e)** 2.5 m **(f)** 3 m

Each experiment starts with 60s of only advective flow (Q) and follows a 60s of advective flow with signal chemicals ($Q+q$). The experiment concludes with 480s of only advective flow (Q). The lengthy advective flow is to clean the sensors from the residual chemicals.

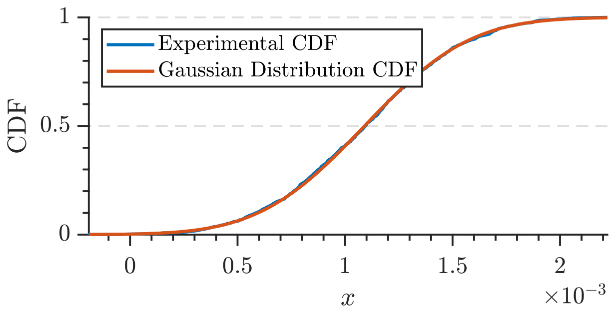

Fig. 8. Experimental results along with a Gaussian fit of the measured noise of the environment

The experiment for each distance was repeated 3 times and a 50 μl sample was injected into the evaporation chamber to refresh the signal chemical in the transmitter.

A. Noise

To analyze the signal-to-noise ratio (SNR), the noise in the communications is measured.

In a study done in [45], the noise present in the communication with a membrane inlet mass spectrometry (MIMS) as a detector was determined to be Additive White Gaussian Noise (AWGN).

TABLE II
PARAMETER USED IN CLOSED BOUNDARY TRANSMISSION

Property	Symbol	Value	Unit
Tracked Signal Ion	m/z	43	Da
Signal Flow	q	8	ml/min
Carrier Flow	Q	750	ml/min
Carrier Flow Pressure	P_Q	1	atm
Vacuum Pump Pressure	P_V	2.4×10^{-6}	torr
Environment Pressure	P_E	1 ± 0.003	bar
Environment Temperature	T_E	297.35 ± 1.5	K
Inner Tube diameter	ϕ_{in}	19.80	mm
Outer Tube diameter	ϕ_{out}	24.25	mm
Acetone detection delay [49]	t_d	15	s
Diffusivity of acetone in air	D_m	0.124	cm^2/s

$$\mathcal{N} = (\mu, \sigma^2) \tag{25}$$

The measured experimental noise along with a Gaussian cumulative distribution function (CDF) fitting can be seen in Figure 8. To quantify the fit, Kolmogorov-Smirnov test is used with the following expression [61].

$$D_n = \sup_x |F_n(x) - F(x)| \tag{26}$$

where $F(x)$ is the measured data and $F_n(x)$ is the theoretically fitted model. As can be seen in the Figure the noise in the system is based on a normal distribution with a D_n value of 0.0114. Based on the fitting, the noise parameters of the communications are:

$$\mu = 1.09 \times 10^{-3} \qquad \sigma^2 = 1.49 \times 10^{-7} \tag{27}$$

B. Transmitted Signal

The experimental results of the closed boundary transmission can be seen in Figure 9. As can be seen, the signal behaves in an irregular fashion and with each consecutive increase in the distance, the signal amplitude decreases and experiences delay in the arrival. The measured detection delay along with the empirical fit can be seen in Figure 6. It must be noted that, the signal retains its shape as the transmission distance increase, showing the possibility of preserving the shape in long distance transmission with loss in only in the signal amplitude.

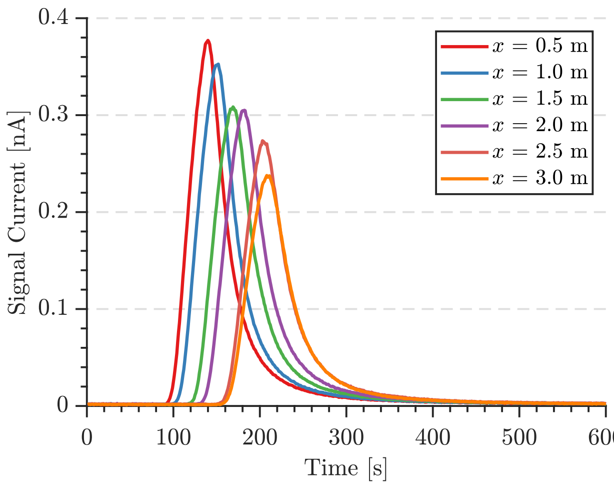

Fig. 9. Experimental results of closed-boundary transmission in macro-scale molecular communications

The comparison of each transmitted signal with its theoretical signal counterpart can be seen in Figure 7 and correlation values (ρ) can be seen in Table III.

TABLE III
CORRELATION VALUES OF THEORETICAL MODEL WITH EXPERIMENTAL DATA

0.5 m	1 m	1.5 m	2 m	2.5 m	3 m
0.9052	0.9170	0.9448	0.8995	0.7685	0.9006

The correlation value is calculated from the Pearson correlation value and the Equation can be seen below.

$$\rho_{E,T} = \frac{\mathrm{cov}(E,T)}{\sigma_E \sigma_T} \tag{28}$$

where E is the experimental data and T is the theoretical data. As can be noted, the theoretically generated signal shows general agreement with the experimentally obtained results. Finally the maximum signal amplitude generated from these transmissions with comparison to the theoretical calculations can be seen in Figure 10a. As can be seen there is some difference between the experimental results and the theoretical model. This difference can be caused by the interactions between the membrane present in the detector and the signal chemical.

C. Signal Energy

As a Mass Spectrometer (MS) measures the amount of particles it detects (M) by ionizing the samples and generating a current, the energy of the signal (β) can be expressed as [30], [45]:

$$\beta(Ł,\, R,\, t) = \int_{-\infty}^{+\infty} |\theta(L,\, R,\, t)|^2 dt \tag{29}$$

where θ is the absorbed/desorption process described in Section III. In this study the energy of the theoretically generated signal is calculated using the following equations. First is the energy generated when the mass is introduced to the system.

$$\begin{aligned}\beta_1(L,\, R,\, t) = \int_{t_{\mathrm{emp}}}^{T_S + t_{\mathrm{emp}}} \Bigg| M - \frac{M}{\mathbf{i}\sqrt{4D_T t}} \\ \times \left[\mathrm{erf}\left(\frac{v_z t}{\sqrt{4D_L t}}\right) + \mathrm{erf}\left(\frac{L - v_z t}{\sqrt{4D_L t}}\right)\right] \\ \sum_{n=0}^{\infty} \exp\left(-n^2 \frac{R^2}{D_T t}\right) \left\{\mathbf{i}\sqrt{D_T t}\left[1 - \exp\left((4n-1)\frac{R^2}{4D_T t}\right)\right] \right. \\ + nR\sqrt{\pi}\exp\left(n^2 \frac{R^2}{D_T t}\right) \\ \left. \times \left[\mathrm{erfi}\left(n\frac{\mathbf{i}R}{\sqrt{D_T t}}\right) - \mathrm{erfi}\left(\frac{(2n-1)}{2}\frac{\mathbf{i}R}{\sqrt{D_T t}}\right)\right]\right\}\Bigg|^2 dt\end{aligned} \tag{30}$$

The second is when the mass is being removed from the detector.

$$\begin{aligned}\beta_0(L_M,\, R,\, t) = \int_{t_{\mathrm{emp}}}^{T_F + t_{\mathrm{emp}}} \Bigg| \frac{M_R}{\mathbf{i}\sqrt{4D_T t}} \\ \times \left[\mathrm{erf}\left(\frac{v_z t}{\sqrt{4D_L t}}\right) + \mathrm{erf}\left(\frac{L_M - v_z t}{\sqrt{4D_L t}}\right)\right] \\ \sum_{n=0}^{\infty} \exp\left(-n^2 \frac{R^2}{D_T t}\right) \left\{\mathbf{i}\sqrt{D_T t}\left[1 - \exp\left((4n-1)\frac{R^2}{4D_T t}\right)\right] \right. \\ + nR\sqrt{\pi}\exp\left(n^2 \frac{R^2}{D_T t}\right) \\ \left. \times \left[\mathrm{erfi}\left(n\frac{\mathbf{i}R}{\sqrt{D_T t}}\right) - \mathrm{erfi}\left(\frac{(2n-1)}{2}\frac{\mathbf{i}R}{\sqrt{D_T t}}\right)\right]\right\}\Bigg|^2 dt\end{aligned} \tag{31}$$

where T_F is the duration of the flush.

$$\begin{aligned}\beta(L;\, L_M,\, R,\, t) = \beta_1(L,\, R,\, t_{\mathrm{emp}} : T_D + t_{\mathrm{emp}}) \\ + \beta_0(L_M,\, R,\, t_{\mathrm{emp}} : T_F + t_{\mathrm{emp}})\end{aligned} \tag{32}$$

The experimental values obtained from this study along with theoretical comparisons can be seen in Figure 10b. As can be seen, the theoretical results of R = 1 cm shows strong

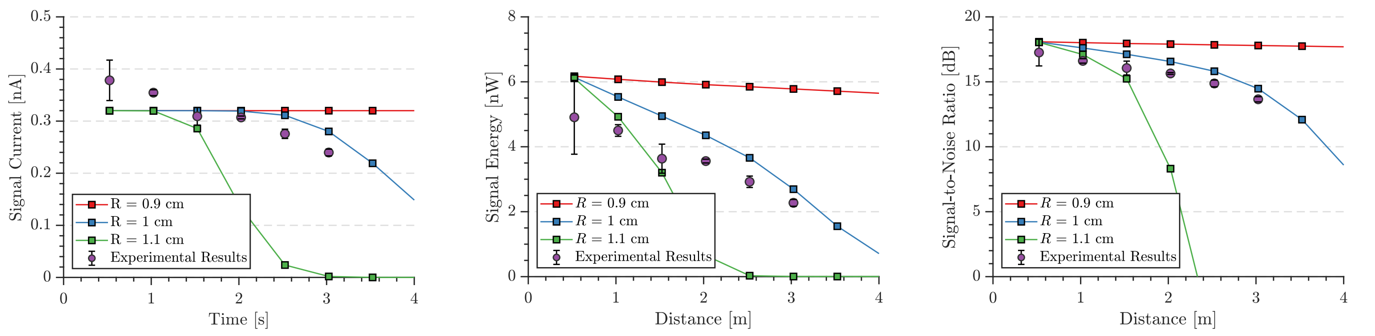

Fig. 10. Experimental along with theoretical comparison of **(a)** Signal Amplitude ($\rho \cong 0.79$) **(b)** Signal Energy ($\rho \cong 0.99$) **(c)** Signal-to-Noise ratio ($\rho \cong 0.99$)

agreement with experimental results ($\rho \cong 0.99$). However, as can be seen in the Figure, there are deviances between the data and the theoretical model. This can be caused by the complex interaction between the membrane and the transmitted signal. Theoretical comparisons of radii 0.9 cm and 1.1 cm can also be seen as well. As is it shown, the small differences in the radius can have a significant impact on the received signal energy. This is due to velocity parameter being inversely proportional to the radius of the transmission medium, shown in Eq. (21).

D. Signal-to-Noise Ratio (SNR)

To calculate the signal to noise ratio, the following equation is used.

$$\mathrm{SNR_{dB}} = 10\log_{10}\left[\frac{\beta\,(L)}{N_0}\right] \tag{33}$$

where N_0 is the energy of the background noise (W) which was measured and shown to behave Gaussian in Section IV-A. The plot of experimental and theoretical comparison as be seen in Figure 10c. As can be seen from the plot the signal experiences an decrease in SNR as the transmission distance increases.

V. Conclusion

This paper presents molecular transmission with radial boundary conditions, analyzed both experimentally and theoretically. To realize the experimental setup, an in-house built gas generator was used as the transmitter and a membrane inlet mass spectrometer (MIMS) with a quadrupole mass analyzer (QMA) was used as the detector. The boundary of the environment in the experimental setup was achieved by utilizing a pipe with an inner diameter of ϕ_{in} = 19.8 mm. To model the propagation a variation of the mass transport equation, known in the literature as advection-diffusion equation derived from the continuity equation, was used. In addition, additional calculations were made in determining the state of the flow and estimation the diffusion coefficient in a confined medium, which was calculated to be laminar. Two types of diffusion coefficients were used, former being parallel to the advective flow (i.e., longitudinal diffusion) and latter being tangential (i.e., transverse diffusion) It was shown that the longitudinal diffusion parameter plays a pivotal role in the behaviour of the propagation in a confined medium compared to transverse diffusion ($D_L \gg D_T$). This is due to the orientation of the advective flow with respect to D_L over D_T.

The experimental results of signal amplitude, signal energy, empirical detection delay and signal-to-noise ratio (SNR) was compared to the theoretical model developed in Section III and was shown to have strong agreement with the experimental data. It was also shown that there is a linear relation between the detection of the signal chemical and the distance it propagates.

Finally theoretical comparison was made to the behaviour of the signal propagation with different radius of the boundary, based on the model. The theoretical study of different radius shows that small changes in the radius parameter has considerable effect on the signal detection time and the signal attenuation.

In the future, simultaneous transmission of multiple chemicals will be investigated along with the effects of Reynold's number on the pipe diameter.

Appendix

A. Derivation of Taylor-Aris Dispersion

It is considered that the flow inside a straight cylindrical pipe is steady, driven by a constant pressure gradient (i.e, Poiseuille flow). The average velocity over the pipe cross-section can be given as:

$$u(r) = 2\overline{u}\left(1 - \frac{r^2}{R^2}\right), \tag{34}$$

where:

$$\overline{u} = \frac{1}{\pi R^2}\int_0^{2\pi} d\,\theta \int_0^R r\,u\,dr. \tag{35}$$

In these equations $\overline{u}$ denotes the average quantity of the velocity flowing through the pipe. If it is assumed that an axisymmetric distribution of material $c(r,\,z,\,t)$ is released into the flow, the evolution of the propagation is described by the ADE in cylindrical form.

$$\frac{\partial c}{\partial t} + u(r)\frac{\partial c}{\partial z} = D_m\left(\frac{\partial^2 c}{\partial z^2} + \frac{1}{r}\frac{\partial}{\partial r}\left(r\frac{\partial c}{\partial r}\right)\right) \tag{36}$$

Since no particle can leave the system, the boundary conditions are same as Eq. (10). By separating c using Reynold's decomposition method,c is separated into its cross-sectional average and r variable parts.

$$c(r,\, z,\, t) = \overline{c}(z,\, t) + c'(r,\, z,\, t), \tag{37}$$

where:

$$\overline{c} = \frac{2}{R^2}\int_0^R rc\, dr. \tag{38}$$

since the average of deviation is zero ($\overline{c'} = 0$) the equation can be written as:

$$\frac{\partial \overline{c}}{\partial t} + \frac{\partial c'}{\partial t} + u(r)\left(\frac{\partial \overline{c}}{\partial z} + \frac{\partial c'}{\partial z}\right) = D_m\left(\frac{\partial^2 \overline{c}}{\partial z^2} + \frac{\partial^2 c'}{\partial z^2} + \frac{1}{r}\frac{\partial}{\partial r}\left(r\frac{\partial c'}{\partial r}\right)\right) \tag{39}$$

Taking the cross-sectional average of Eq. (39) yields the following simplification taking into account that $\partial c'/\partial t = 0$ on $r = R$.

$$\frac{\partial \overline{c}}{\partial t} + \overline{u(r)}\frac{\partial \overline{c}}{\partial z} + \overline{u(r)\frac{\partial c'}{\partial z}} = D_m\frac{\partial^2 \overline{c}}{\partial z^2} \tag{40}$$

The the mean concentration $\overline{c}$ depends on the average advection of the r-varying part of c (i.e., $c'(r,\, z,\, t)$), which is calculated by subtracting Eq. (40) from Eq. (39) reveals the r-varying component of Eq. (39),

$$\frac{\partial c'}{\partial t} + (u(r) - \overline{u})\frac{\partial \overline{c}}{\partial z} + u\frac{\partial c'}{\partial z} - \overline{u\frac{\partial c'}{\partial z}} = D_m\nabla^2 c' \tag{41}$$

Based on this equation, an approximation is made whereby after a time of in the order $t = R^2/D_m$ the radial diffusion to have almost smoothed out variation in the r-axis. Thus for $t \sim \mathcal{O}\left(R^2/D_m\right)$, it is expected for $\overline{c} \gg c'$. In addition, the gradients in the r-direction are greater than those in the z-direction. Therefore the primary balance is:

$$(u(r) - \overline{u})\frac{\partial \overline{c}}{\partial z} \simeq \frac{D_m}{r}\frac{\partial}{\partial r}\left(r\frac{\partial c'}{\partial r}\right) \tag{42}$$

Introducing Eq. (34) into (42), the following expression is derived.

$$\frac{\partial}{\partial r}\left(r\frac{\partial c'}{\partial r}\right) = \frac{\overline{u}}{D_m}\frac{\partial \overline{c}}{\partial z}\left(r - \frac{2r^3}{R^2}\right) \tag{43}$$

As shown in the Reynold's decomposition of c in Eq. (37), $\overline{c}$ is independent from r, so Eq. (43) can be integrated twice over,

$$c' = \frac{\overline{u}}{D_m}\frac{\partial \overline{c}}{\partial z}\left(\frac{r^2}{4} - \frac{r^4}{8R^2} + A + B\ln r\right) \tag{44}$$

Since c' is regular at $r = 0$ B can be declared the value of 0. Furthermore, c' has zero average. This yields:

$$\int_0^R r u' dr = 0, \tag{45}$$

This equation give A the value of:

$$A = -\frac{R^2}{12} \tag{46}$$

$$c' = \frac{\overline{u}R_r^2}{24D_m}\frac{\partial \overline{c}}{\partial z}\left(6R_r^2 - 3R_r^4 - 2\right) \quad \text{where} \quad R_r = \frac{r}{R} \tag{47}$$

Equation (4) requires the term $\overline{u(r)\partial c'/\partial z}$, which is

$$\overline{u(r)\frac{\partial c'}{\partial z}} = -\frac{R^2\overline{u}}{48D_m}\frac{\partial^2 \overline{c}}{\partial z^2} \tag{48}$$

Substituting this result into Eq. (40), ADE for the mean concentration $\overline{c}(z, t)$ is derived.

$$\frac{\partial \overline{c}}{\partial t} + \overline{u}\frac{\partial \overline{c}}{\partial z} = \left(D_m + \frac{R^2\overline{u}^2}{48D_m}\right)\frac{\partial^2 \overline{c}}{\partial z^2} = D_{\text{eff}}\frac{\partial^2 \overline{c}}{\partial z^2} \tag{49}$$

REFERENCES

[1] Z. Sun and I. F. Akyildiz, "Underground wireless communication using magnetic induction," in *2009 IEEE International Conference on Communications*. IEEE, 2009, pp. 1–5.

[2] L. Lanbo, Z. Shengli, and C. Jun-Hong, "Prospects and problems of wireless communication for underwater sensor networks," *Wireless Communications and Mobile Computing*, vol. 8, no. 8, pp. 977–994, 2008.

[3] I. F. Akyildiz and E. P. Stuntebeck, "Wireless underground sensor networks: Research challenges," *Ad Hoc Networks*, vol. 4, no. 6, pp. 669–686, 2006.

[4] T. Nakano, A. W. Eckford, and T. Haraguchi, *Molecular communication*. Cambridge University Press, 2013.

[5] W. Guo, C. Mias, N. Farsad, and J.-L. Wu, "Molecular versus electromagnetic wave propagation loss in macro-scale environments," *IEEE Transactions on Molecular, Biological and Multi-Scale Communications*, vol. 1, no. 1, pp. 18–25, 2015.

[6] R. A. Bradshaw and E. A. Dennis, *Handbook of cell signaling*. Academic press, 2009.

[7] A. B., J. A., L. J., R. M., R. K., and W. P., *Molecular Biology of the Cell* 5^{th} *edition (New York: Garland Science)*, 2007.

[8] W. R. Loewenstein, "On the genesis of cellular communication," *Developmental biology*, vol. 15, no. 6, pp. 503–520, 1967.

[9] R. J. Linhardt and T. Toida, "Role of glycosaminoglycans in cellular communication," *Accounts of chemical research*, vol. 37, no. 7, pp. 431–438, 2004.

[10] W. C. Agosta, *Chemical communication: the language of pheromones*. Henry Holt and Company, 1992.

[11] R. K. Vander Meer, M. D. Breed, K. E. Espelie, and M. L. Winston, "Pheromone communication in social insects," *Ants, wasps, bees and termites. Westview, Boulder, CO*, vol. 162, 1998.

[12] K. N. Slessor, M. L. Winston, and Y. Le Conte, "Pheromone communication in the honeybee (apis mellifera l.)," *Journal of chemical ecology*, vol. 31, no. 11, pp. 2731–2745, 2005.

[13] A. E. Forooshani, S. Bashir, D. G. Michelson, and S. Noghanian, "A survey of wireless communications and propagation modeling in underground mines," *IEEE Communications surveys & tutorials*, vol. 15, no. 4, pp. 1524–1545, 2013.

[14] M. Stojanovic, "Acoustic (underwater) communications," *Wiley Encyclopedia of Telecommunications*, 2003.

[15] M. Cole, J. Gardner, S. Pathak, T. Pearce, and Z. Rácz, "Towards a biosynthetic infochemical communication system," *Procedia Chemistry*, vol. 1, no. 1, pp. 305–308, 2009.

[16] L. Muñoz, N. Dimov, G. Carot-Sans, W. P. Bula, A. Guerrero, and H. J. Gardeniers, "Mimicking insect communication: Release and detection of pheromone, biosynthesized by an alcohol acetyl transferase immobilized in a microreactor," *PloS one*, vol. 7, no. 11, p. e47751, 2012.

[17] M. Cole, J. Gardner, Z. Ráczu, S. Pathak, T. Pearce, J. Challiss, D. Markovic, A. Guerrero, L. Muñoz, G. Carot *et al.*, "Biomimetic insect infochemical communication system," in *Sensors, 2009 IEEE*. IEEE, 2009, pp. 1358–1361.

[18] R. A. Russell, "An odour sensing robot draws inspiration from the insect world," in *Bioelectromagnetism, 1998. Proceedings of the 2nd International Conference on*. IEEE, 1998, pp. 49–50.

[19] ——, *Odour detection by mobile robots*. World Scientific, 1999, vol. 22.

[20] M. S. Kuran, H. B. Yilmaz, T. Tugcu, and I. F. Akyildiz, "Modulation techniques for communication via diffusion in nanonetworks," in *Communications (ICC), 2011 IEEE International Conference on*. IEEE, 2011, pp. 1–5.

[21] M. Ş. Kuran, H. B. Yilmaz, T. Tugcu, and I. F. Akyildiz, "Interference effects on modulation techniques in diffusion based nanonetworks," *Nano Communication Networks*, vol. 3, no. 1, pp. 65–73, 2012.

[22] M. U. Mahfuz, D. Makrakis, and H. T. Mouftah, "On the characterization of binary concentration-encoded molecular communication in nanonetworks," *Nano Communication Networks*, vol. 1, no. 4, pp. 289–300, 2010.

[23] B. Krishnaswamy, C. M. Austin, J. P. Bardill, D. Russakow, G. L. Holst, B. K. Hammer, C. R. Forest, and R. Sivakumar, "Time-elapse communication: Bacterial communication on a microfluidic chip," *IEEE Transactions on Communications*, vol. 61, no. 12, pp. 5139–5151, 2013.

[24] Y.-P. Hsieh, Y.-C. Lee, P.-J. Shih, P.-C. Yeh, and K.-C. Chen, "On the asynchronous information embedding for event-driven systems in molecular communications," *Nano Communication Networks*, vol. 4, no. 1, pp. 2–13, 2013.

[25] N. Garralda, I. Llatser, A. Cabellos-Aparicio, E. Alarcón, and M. Pierobon, "Diffusion-based physical channel identification in molecular nanonetworks," *Nano Communication Networks*, vol. 2, no. 4, pp. 196–204, 2011.

[26] N.-R. Kim and C.-B. Chae, "Novel modulation techniques using isomers as messenger molecules for nano communication networks via diffusion," *IEEE Journal on Selected Areas in Communications*, vol. 31, no. 12, pp. 847–856, 2013.

[27] N. Farsad, W. Guo, and A. W. Eckford, "Tabletop molecular communication: Text messages through chemical signals," *PloS one*, vol. 8, no. 12, p. e82935, 2013.

[28] S. Giannoukos, D. Tunç McGuiness, A. Marshall, J. Smith, and S. Taylor, "A chemical alphabet for macromolecular communications." *Analytical Chemistry*, vol. 0, no. ja, p. null, 0, pMID: 29847932. [Online]. Available: https://doi.org/10.1021/acs.analchem.8b01716

[29] L. Grebenstein, J. Kirchner, R. S. Peixoto, W. Zimmermann, W. Wicke, A. Ahmadzadeh, V. Jamali, G. Fischer, R. Weigel, A. Burkovski *et al.*, "Biological optical-to-chemical signal conversion interface: a small-scale modulator for molecular communications," in *Proceedings of the 5th ACM International Conference on Nanoscale Computing and Communication*. ACM, 2018, p. 29.

[30] D. T. McGuiness, S. Giannoukos, A. Marshall, and S. Taylor, "Parameter analysis in macro-scale molecular communications using advection-diffusion," *IEEE Access*, 2018.

[31] M. Pierobon and I. F. Akyildiz, "Noise analysis in ligand-binding reception for molecular communication in nanonetworks," *IEEE Transactions on Signal Processing*, vol. 59, no. 9, pp. 4168–4182, 2011.

[32] T. Nakano, Y. Okaie, and J.-Q. Liu, "Channel model and capacity analysis of molecular communication with brownian motion," *IEEE communications letters*, vol. 16, no. 6, pp. 797–800, 2012.

[33] M. Pierobon and I. F. Akyildiz, "Diffusion-based noise analysis for molecular communication in nanonetworks," *IEEE Transactions on Signal Processing*, vol. 59, no. 6, pp. 2532–2547, 2011.

[34] B. Atakan, "Optimal transmission probability in binary molecular communication," *IEEE Communications Letters*, vol. 17, no. 6, pp. 1152–1155, 2013.

[35] D. Arifler, "Capacity analysis of a diffusion-based short-range molecular nano-communication channel," *Computer Networks*, vol. 55, no. 6, pp. 1426–1434, 2011.

[36] A. Einolghozati, M. Sardari, A. Beirami, and F. Fekri, "Capacity of discrete molecular diffusion channels," in *Information Theory Proceedings (ISIT), 2011 IEEE International Symposium on*. IEEE, 2011, pp. 723–727.

[37] A. Einolghozati, M. Sardari, and F. Fekri, "Capacity of diffusion-based molecular communication with ligand receptors," in *Information Theory Workshop (ITW), 2011 IEEE*. IEEE, 2011, pp. 85–89.

[38] B. Atakan and O. B. Akan, "Deterministic capacity of information flow in molecular nanonetworks," *Nano Communication Networks*, vol. 1, no. 1, pp. 31–42, 2010.

[39] J. G. Kirkwood, R. L. Baldwin, P. J. Dunlop, L. J. Gosting, and G. Kegeles, "Flow equations and frames of reference for isothermal diffusion in liquids," *The Journal of Chemical Physics*, vol. 33, no. 5, pp. 1505–1513, 1960.

[40] H. Li, S. M. Moser, and D. Guo, "Capacity of the memoryless additive inverse gaussian noise channel," *IEEE Journal on Selected Areas in Communications*, vol. 32, no. 12, pp. 2315–2329, 2014.

[41] H. ShahMohammadian, G. G. Messier, and S. Magierowski, "Nano-machine molecular communication over a moving propagation medium," *Nano Communication Networks*, vol. 4, no. 3, pp. 142–153, 2013.

[42] D. T. McGuiness, S. Giannoukos, A. Marshall, and S. Taylor, "Modulation analysis in macro-molecular communications," *IEEE Access*, 2019.

[43] D. T. McGuiness, V. Selis, and A. Marshall, "Molecular-based nano-communication network: a ring topology nano-bots for in-vivo drug delivery systems," *IEEE Access*, 2019.

[44] R. P. Feynman, R. B. Leighton, and M. Sands, *The Feynman lectures on physics, Vol. I: The new millennium edition: mainly mechanics, radiation, and heat*. Basic books, 2011, vol. 1.

[45] D. T. McGuiness, S. Giannoukos, A. Marshall, and S. Taylor, "Experimental results on the open-air transmission of macro-molecular communication using membrane inlet mass spectrometry," *IEEE Communications Letters*, pp. 1–1, 2018.

[46] W. J. Lucas, A. Groover, R. Lichtenberger, K. Furuta, S.-R. Yadav, Y. Helariutta, X.-Q. He, H. Fukuda, J. Kang, S. M. Brady *et al.*, "The plant vascular system: evolution, development and functionsf," *Journal of integrative plant biology*, vol. 55, no. 4, pp. 294–388, 2013.

[47] M. Statheropoulos, G. Pallis, K. Mikedi, S. Giannoukos, A. Agapiou, A. Pappa, A. Cole, W. Vautz, and C. P. Thomas, "Dynamic vapor generator that simulates transient odor emissions of victims entrapped in the voids of collapsed buildings," *Analytical chemistry*, vol. 86, no. 8, pp. 3887–3894, 2014.

[48] D. McGuiness, A. Marshall, S. Taylor, and S. Giannoukos, "Asymmetrical inter-symbol interference in macro-scale molecular communications," in *Proceedings of the 5th ACM International Conference on Nanoscale Computing and Communication*. ACM, 2018, p. 13.

[49] S. Giannoukos, A. Marshall, S. Taylor, and J. Smith, "Molecular communication over gas stream channels using portable mass spectrometry," *Journal of The American Society for Mass Spectrometry*, vol. 28, no. 11, pp. 2371–2383, 2017.

[50] E. De Hoffmann, "Mass spectrometry," *Kirk-Othmer Encyclopedia of Chemical Technology*, 2000.

[51] S. Giannoukos, B. Brkić, S. Taylor, and N. France, "Membrane inlet mass spectrometry for homeland security and forensic applications," *Journal of the American Society for Mass Spectrometry*, vol. 26, no. 2, pp. 231–239, 2015.

[52] S. Maher, F. Jjunju, I. Young, B. Brkic, and S. Taylor, "Membrane inlet mass spectrometry for in situ environmental monitoring," *Spectrosc. Eur*, vol. 26, pp. 6–8, 2014.

[53] S. Giannoukos, B. Brkicé, S. Taylor, and N. France, "Monitoring of human chemical signatures using membrane inlet mass spectrometry," *Analytical chemistry*, vol. 86, no. 2, pp. 1106–1114, 2013.

[54] S. Giannoukos, B. Brkicé, S. Taylor, A. Marshall, and G. F. Verbeck, "Chemical sniffing instrumentation for security applications," *Chemical reviews*, vol. 116, no. 14, pp. 8146–8172, 2016.

[55] S. Giannoukos, B. Brkić, and S. Taylor, "Analysis of chlorinated hydrocarbons in gas phase using a portable membrane inlet mass spectrometer," *Analytical Methods*, vol. 8, no. 36, pp. 6607–6615, 2016.

[56] R. A. Ketola and F. R. Lauritsen, "Membrane inlet mass spectrometry (mims) in historical perspective," in *The Encyclopedia of Mass Spectrometry*. Elsevier, 2016, pp. 143–148.

[57] J. Pedlosky, *Geophysical fluid dynamics*. Springer Science & Business Media, 2013.

[58] T. Stocker, *Introduction to climate modelling*. Springer Science & Business Media, 2011.

[59] J. Crank *et al.*, *The mathematics of diffusion*. Oxford university press, 1979.

[60] A. Sommerfeld, "Ein beitrag zur hydrodynamischen erklaerung der turbulenten fluessigkeitsbewegungen," *Atti del*, vol. 4, pp. 116–124, 1908.

[61] W. W. Daniel *et al.*, *Applied nonparametric statistics*. Houghton Mifflin, 1978.